European Radiology (2019) 29:5322–5329
https://doi.org/10.1007/s00330-019-06183-y

CARDIAC

Deep learning–based image restoration algorithm for coronary CT angiography

Fuminari Tatsugami[1] · Toru Higaki[1] · Yuko Nakamura[1] · Zhou Yu[2] · Jian Zhou[2] · Yujie Lu[2] · Chikako Fujioka[3] · Toshiro Kitagawa[4] · Yasuki Kihara[4] · Makoto Iida[1] · Kazuo Awai[1]

Received: 21 August 2018 / Revised: 9 March 2019 / Accepted: 19 March 2019 / Published online: 8 April 2019

Abstract

Objectives The purpose of this study was to compare the image quality of coronary computed tomography angiography (CTA) subjected to deep learning–based image restoration (DLR) method with images subjected to hybrid iterative reconstruction (IR).

Methods We enrolled 30 patients (22 men, 8 women) who underwent coronary CTA on a 320-slice CT scanner. The images were reconstructed with hybrid IR and with DLR. The image noise in the ascending aorta, left atrium, and septal wall of the ventricle was measured on all images and the contrast-to-noise ratio (CNR) in the proximal coronary arteries was calculated. We also generated CT attenuation profiles across the proximal coronary arteries and measured the width of the edge rise distance (ERD) and the edge rise slope (ERS). Two observers visually evaluated the overall image quality using a 4-point scale (1 = poor, 4 = excellent).

Results On DLR images, the mean image noise was lower than that on hybrid IR images (18.5 ± 2.8 HU vs. 23.0 ± 4.6 HU, $p < 0.01$) and the CNR was significantly higher ($p < 0.01$). The mean ERD was significantly shorter on DLR than on hybrid IR images, whereas the mean ERS was steeper on DLR than on hybrid IR images. The mean image quality score for hybrid IR and DLR images was 2.96 and 3.58, respectively ($p < 0.01$).

Conclusions DLR reduces the image noise and improves the image quality at coronary CTA.

Key Points

- *Deep learning–based image restoration is a new technique that employs the deep convolutional neural network for image quality improvement.*
- *Deep learning–based restoration reduces the image noise and improves image quality at coronary CT angiography.*
- *This method may allow for a reduction in radiation exposure.*

Keywords Computed tomography angiography · Cardiac imaging techniques · Artificial intelligence · Image enhancement

Abbreviations

CNR	Contrast-to-noise ratio
CTA	Computed tomography angiography
DCNN	Deep convolutional neural network
DLR	Deep learning–based image restoration
ERD	Edge rise distance
ERS	Edge rise slope

Introduction

Coronary computed tomography angiography (CTA) is a robust noninvasive imaging technique with high spatial and temporal resolution. Its diagnostic accuracy is high for the exclusion of coronary artery disease [1–3]. However, some factors such as high image noise, insufficient vessel enhancement, and blooming- and beam-hardening artifacts may hamper the precise evaluation of vessel stenosis.

Artificial intelligence (AI) is of interest due to its potential to improve the reconstruction of CT images [4, 5]. AI, and more specifically, deep-learning systems facilitate an end-to-

✉ Fuminari Tatsugami
sa104@rg8.so-net.ne.jp

[1] Department of Diagnostic Radiology, Hiroshima University, 1-2-3 Kasumi, Minami-ku, Hiroshima 734-8551, Japan

[2] Canon Medical Research USA, Inc., 706 N Deerpath Drive, Vernon Hills, IL 60061, USA

[3] Department of Radiology, Hiroshima University, 1-2-3 Kasumi, Minami-ku, Hiroshima 734-8551, Japan

[4] Department of Cardiovascular Medicine, Hiroshima University, 1-2-3 Kasumi, Minami-ku, Hiroshima 734-8551, Japan

end approach by learning simple features as components of more complex features such as shapes, lesions, or organs [6]. Several clinical applications of this technique have been proposed in the field of radiology for lesion classification [7], lesion detection [8, 9], and organ segmentation [10]. Deep learning has been used mainly for computer-assisted detection and diagnosis. Recently, the usefulness of AI for improving the reconstruction of CT images and for image-space-based reconstruction, in which convolutional neural networks are trained on low-dose- to reconstruct routine-dose CT images, has been investigated [11, 12].

We developed a CT image restoration technique, a deep learning–based image restoration (DLR) method, which incorporates a noise and artifact reduction filter by the deep convolutional neural network (DCNN). Our network was trained with noise-contaminated and noise-free training pairs to allow the network to extract signals from noisy images. To our knowledge, no study has evaluated the quality of coronary CTA images using a DCNN-based method. The purpose of this study was to compare the image quality of coronary CTA scans reconstructed with DLR or hybrid iterative reconstruction (IR) (adaptive iterative dose reduction 3D: AIDR 3D, Canon Medical Systems Corp.).

Materials and methods

Deep learning–based image restoration

Deep learning–based image restoration (DLR) is the latest application that incorporates a convolution neural network kernel after the image reconstruction process (Fig. 1). The neural network module was trained to extract signal from low-dose hybrid IR images to have similar image quality as the high-dose model-based IR (MBIR) target. During the training process, both noise-contaminated and noise-free training samples were provided to the network as training pairs, so that the network can learn the difference between signal and noise. The network is used to incorporate advanced physics models (e.g., statistical model, scanner model, optics model, cone angle model) into this method through learning from the target images, which had been carefully considered and estimated in the MBIR target image. Details of DCNN structure and parameters are described as follows.

DLR training process

The training process for DLR is carefully designed to map training input $\boldsymbol{X}$ to desired target $\boldsymbol{Y}$, as shown in Fig. 2. This training process can be described as solving the following optimization problem:

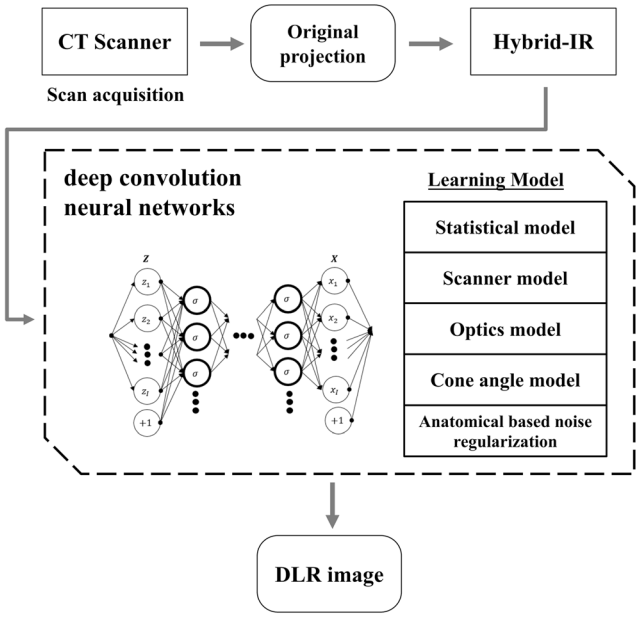

Fig. 1 Schematic drawing of deep learning–based image restoration process

$$\Theta^{*} = \operatorname{argmin} \frac{1}{N} \sum_{i=1}^{N} \|f(x_i;\Theta) - y_i\|^2$$

where Θ is the set of parameters of the neural network to be optimized, N is the total number of training instances in training process, f is the neural network to be optimized, x_i is the ith element of the training input, and y_i is the ith element of the training target. By solving this optimization problem, one can find the optimal network parameter Θ^{*}, such that the difference between the network output and the target image Y will be minimized. This optimization problem is solved iteratively using the ADAM algorithm with gradually decreased learning rate to 10^{-5}, and the loss function can reach a static value after 60 epochs in this study. A ten-layer linear residual network with common CNN components like convolution layer, batch normalization layer, and RELU activation function was applied in this research (Fig. 3). All CNN training computations were processed in the MatConvNet software (ver. 1.0, VLFeat.org).

DLR training and validation data sets

The training target data set comprised clinical high-quality cardiac 120-kVp scans (700–750 mA, 0.275 s/round), which was acquired with a target SD index from 22.0 to 27.5. MBIR algorithm was used for achieving the best possible image resolution and noise suppression performance images. For getting better generalizability of the network, we augment the data set by creating several simulated low-dose noisy scans. To do this, simulated noise through the statistical model tool including both quantum noise and electronic noise that

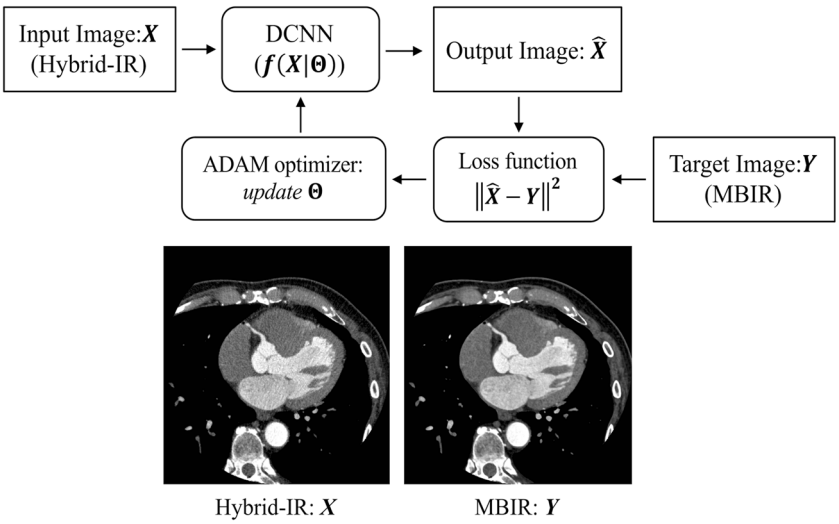

Fig. 2 The neural network training process for deep learning–based image restoration

corresponds to 12.5%, 25%, 50%, and 75% of the original dose was added to the training sets [13]. This way enables the effective dose in the training pool to cover from 87.5 to 563 mA (average 299.7 mA, STDEV 179.8 mA) is enabled. Besides, to handle different noise correlation across different images, the training input is further augmented by reconstructing the clinical data and simulated low-dose data using with different reconstruction field of view (FOV) of 100, 150, 200, 250, and 320 mm to cover most clinical relevant FOV sizes for the cardiac scan. Reconstructing input at different FOVs allows the network to learn the noise texture and noise correlation at different FOVs. All training input data were reconstructed with default hybrid IR algorithm in the scanner (AIDR 3D, Canon Medical Systems Corp.). All input and target images were reconstructed in 512 by 512 pixel size. Overall, more than 100,000 training patches were used in the DLR training process; Fig. 4 shows 5 representative training input and target images of different scan conditions and reconstruction FOVs.

Patients

Institutional review board approval was obtained for this retrospective study; informed consent was waived. We enrolled 30 patients (22 men, 8 women; median age 69 years; range 41–84 years) who underwent coronary CTA between February 2015 and December 2017. In 21 patients, coronary artery disease (CAD) was suspected due to typical angina

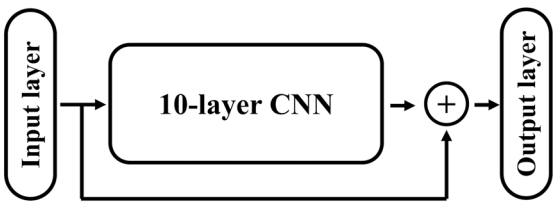

Fig. 3 Deep convolution residual neural network module. "conv" abbreviates for convolution, "RELU" represents rectified linear unit, and "BN" represents batch normalization layer

10-layer CNN module	Kernel size	Input channel	Output channel
1st conv layer + RELU	7 × 7	1	64
2nd conv layer + BN +RELU	3 × 3	64	64
3rd conv layer + BN +RELU	7 × 7	64	64
4th conv layer + BN +RELU	7 × 7	64	64
5th conv layer + BN +RELU	7 × 7	64	64
6th conv layer + BN +RELU	7 × 7	64	64
7th conv layer + BN +RELU	7 × 7	64	64
8th conv layer + BN +RELU	7 × 7	64	64
9th conv layer + BN +RELU	3 × 3	64	64
10th conv layer + BN +RELU	3 × 3	64	1

	a	b	c	d	e
Target image MBIR	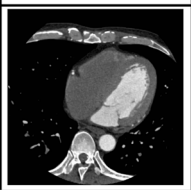			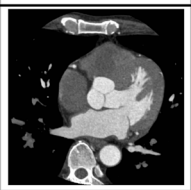	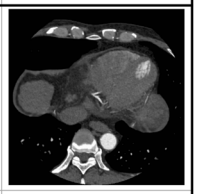
Target dose (mA)	700	700	700	700	700
Input image Hybrid-IR	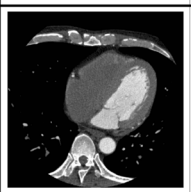		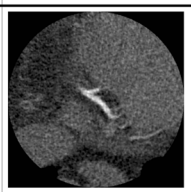	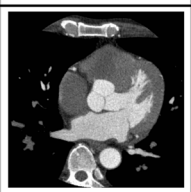	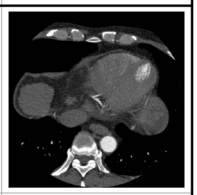
Input dose (mA)	700	87.5	175	350	525
FOV (mm)	250	150	100	200	250

Fig. 4 Representative training input and target images with different dose level and reconstructed field of view (FOV)

pectoris ($n = 9$), atypical chest pain ($n = 5$), dyspnea ($n = 4$), or high cardiovascular risks ($n = 3$). The other 9 had known CAD; they were referred for stent patency ($n = 7$) or follow-up after myocardial infarction ($n = 2$). Our exclusion criteria were renal insufficiency (estimated glomerular filtration rate < 30 ml/min per 1.73 m^2), allergy to contrast agents, a history of bypass grafting, and potential pregnancy.

CT scanning

All CT scans were performed on a 320-detector row CT scanner (Aquilion ONE Vision; Canon Medical Systems Corp.). Patients with a resting heart rate exceeding 65 beats per minute (bpm) received 20–40 mg of metoprolol (Selokeen; AstraZeneca) perorally 60 min before the CT studies. All patients were given one dose of nitroglycerin (Myocor; Astellas Pharma) as a sublingual spray (0.3 mg) approximately 5 min before the examination to dilate the coronary arteries.

The contrast material volume was adapted to the body weight. Using a power injector (DUAL SHOT GX7; Nemoto Kyorindo), we delivered 210 mgI/kg of nonionic contrast material (Iomeprol, Iomeron 350 mgI/ml; Eisai) at a fixed duration of 10 s to all patients. Then, 30 ml of a 0.9% saline solution was injected at the same flow rate as the contrast material. The scan delay was determined with an automatic bolus tracking system (SURE Start Technique; Canon). The scan parameters were collimation, 320 × 0.5 mm; rotation time, 0.275 s; z-coverage, 120–160 mm; tube voltage, 100 or 120 kV; and tube current, 430–750 mA. All examinations were performed with ECG triggering; the phase window during which the patient was exposed was limited to 70–80% of the cardiac cycle (heart rate < 65 bpm) or to 40–80% (heart rate > 65 bpm). Dose modulation was used in patients whose myocardial or valve motion had to be observed throughout the cardiac cycle.

In each patient, the reconstruction phase with minimum artifacts was determined at the CT console using cardiac-phase search software (PhaseXact; Canon). Axial images were reconstructed; the slice thickness and reconstruction interval were 0.5 mm. The image reconstruction field of view was 160–200 mm; the matrix size was 512 × 512. All images were reconstructed with the hybrid IR algorithm (AIDR 3D, Canon Medical Systems Corp.) at standard settings using a medium sharp kernel (FC14) and with DLR. Reconstructed image data were transferred to a workstation (Virtual Place version 3.3; Aze) for post-processing.

The CT dose index ($CTDI_{vol}$) and dose-length product (DLP) provided by the CT scanner were recorded for each patient. The effective radiation dose was calculated as the product of the DLP multiplied by a conversion coefficient for the chest ($k = 0.014$ mSv/mGycm) [14].

Quantitative analysis

One board-certified radiologist with 11 years of experience in cardiac radiology collected all measurements. The contrast-to-noise ratio (CNR) and the margin sharpness at the proximal coronary arteries were assessed on both hybrid IR and DLR images.

Image noise For each of the two reconstruction methods, the image noise was recorded as the standard deviation (SD) of the attenuation value in a circular region of interest (ROI) that

was placed in the ascending aorta, left atrium, and septal wall of the ventricle (Fig. 5).

Contrast-to-noise ratio We calculated the CNR in the proximal right and left main coronary arteries (RCA, LMA) [15, 16]. First, attenuation in an ROI in the proximal RCA and the LMA was measured. The vessel contrast was calculated as the difference in mean attenuation between the contrast-enhanced vessel lumen and the adjacent perivascular tissue. All ROI measurements were performed on axial images; calcifications, plaques, and stenosis were carefully avoided. Then the CNR was calculated as the ratio of the vessel contrast over the image noise in the ascending aorta.

Margin sharpness of the coronary arteries We generated CT attenuation profiles along a horizontal line through the lumen center of the proximal RCA and LMA. ImageJ software (National Institutes of Health, Bethesda, MD) (http://rsb.info.nih.gov/ij) and its particle analysis tool (Plot Profile) were used to generate the profile curves. Again, calcifications and plaques were carefully avoided. CT attenuation profiles were generated at precisely the same location for images reconstructed with hybrid IR and DLR. Then we measured the width of the edge response at the boundary of the proximal coronary arteries determined by the 10–90% edge rise distance (ERD), and calculated the edge rise slope (ERS) (ERS = $(CT_{90\%} - CT_{10\%})$/ERD) [17]. The ERD and ERS were examined on both sides of the coronary arteries and the mean values (ERD_{mean}, ERS_{mean}) were recorded and compared for hybrid IR and DLR images.

Qualitative analysis

On the workstation, a CT technologist with 9 years of experience performed curved multiplanar reconstruction of the three major branches (right coronary, left anterior descending coronary, and left circumflex coronary artery (RCA, LAD, LCX)) from the proximal to the distal segment on both hybrid IR and DLR images. All images were presented in random order for image quality evaluation.

A board-certified radiologist and a cardiologist with 11 and 6 years of experience in cardiac radiology, respectively, assessed the overall image quality for each major branch of the coronary arteries. The readers were blinded to clinical information and the reconstruction method. If their data analysis disagreed, a final decision was reached by consensus. The overall image quality of each coronary artery segment was rated on a 4-point rating score for each coronary artery segment (4 = excellent (minimal or no noise-related blurring, diagnostic information sufficient); 3 = good (some noise-related blurring, diagnostic information acceptable); 2 = fair (marked noise-related blurring, diagnostic information limited); 1 = poor (blurry, diagnostic information impaired)). Images with a score of 3 or 4 were considered diagnostic.

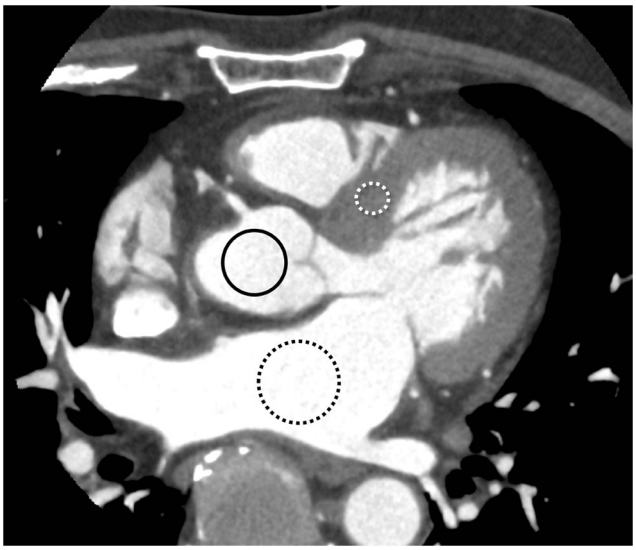

Fig. 5 Enhancement values for the ascending aorta (black line), left atrium (dotted black line), and septal wall of the ventricle (dotted white line) were measured using a circular region of interest (ROI) cursor

Statistical analyses

We performed all statistical tests with Med-Calc software (version 11.3.7.0, MedCalc). Differences were considered to be statistically significant at $p < 0.05$. The image noise, CNR, ERD, and ERS were compared on images reconstructed with hybrid IR and with DLR using the paired t test. The image quality score of the coronary arteries on the two image data sets was compared using the Wilcoxon signed-rank test. Interobserver agreement in the qualitative evaluation was assessed with the Cohen kappa κ coefficient where a κ value of less than 0.20 = poor, 0.21–0.40 = fair, 0.41–0.60 = moderate, 0.61–0.80 = substantial, and 0.81–1.00 = near-perfect agreement.

Results

All CT scans were acquired without complications. The mean body mass index of our patients was 24.5 ± 3.9 (range 18.1–37.3); their mean heart rate during scanning was 53.6 ± 6.1 bpm (median 54 bpm, range 38–68 bpm). All examinations were performed within a single heartbeat. Of the 30 patients, 21 underwent imaging with prospective ECG gating, the other 9 were imaged with a dose modulation. The mean effective radiation dose was 5.4 ± 2.2 mSv (range, 2.3–9.0 mSv).

At each site measured, the mean image noise was significantly lower on DLR than hybrid IR images; the CNR in the proximal coronary arteries was significantly higher on DLR

than on hybrid IR images (Table 1). The mean ERD was significantly shorter on DLR than on hybrid IR images; the mean ERS was significantly steeper on DLR than on hybrid IR images (Table 2).

In both two-volume data sets, a total of 90 major coronary branches were available for evaluation. The results of visual evaluation of the coronary arteries on hybrid IR and DLR images are shown in Table 3. The overall image quality was significantly better on DLR images ($p < 0.01$); the mean image quality score for hybrid IR and DLR images was 2.96 and 3.58, respectively. There was substantial interobserver agreement with respect to the overall image quality ($\kappa = 0.77$). A representative case is shown in Fig. 6.

Discussion

Ours is the first study to evaluate the effect of DLR on the image quality of coronary arteries. On DLR images, the image noise was lower and the coronary artery margins were sharper than those on hybrid IR images.

The principle underlying the DLR noise reduction process is different from the conventional convolution filter approach. When noisy data are used as the training input and high-quality data are presented as the training target, the network can learn to produce clean from noise-contaminated images. Our training target data set for DLR was comprised of high-quality MBIR images. The spatial resolution is higher on MBIR than on conventional filtered back projection (FBP) and hybrid-IR images [18, 19]. The sophisticated modeling of MBIR has been reported to reduce blooming artifacts and to yield a better image quality than hybrid IR [17]. Consequently, we hypothesized that DLR images would exhibit the advantages of MBIR imaging, e.g., image noise reduction and better spatial resolution. Indeed, DLR imaging yielded a higher image quality than conventional hybrid IR.

In our image-quality assessment, we compared DLR with hybrid IR images. As our method reduced the image noise by approximately 20% and improved the image quality, its application may allow for a radiation dose reduction at coronary CTA with prospective ECG triggering. As the image noise is inversely related to the square root of the tube current [20], theoretically, it may be possible to reduce radiation exposure by up to 36% at coronary CTA. Studies are underway to determine whether diagnostic accuracy is retained at reduced radiation doses.

The mean ERD was significantly shorter on DLR than on hybrid IR images, while the mean ERS was significantly steeper on DLR than on hybrid-IR images. A shorter ERD and a steeper ERS result in sharper edges [21]. Consequently, the image quality of the coronary arteries was significantly improved by DLR. It has been reported that the edge is sharper on MBIR than on images reconstructed with conventional FBP or hybrid IR [17, 22]. DLR had a similar effect on the boundary of the coronary arteries. Although we did not assess its diagnostic accuracy by comparing our findings with the reference standard for invasive coronary angiography, we expect that the routine use of DLR will result in better diagnostic accuracy than conventional hybrid IR imaging in patients with suspected CAD.

DLR improved the image quality of coronary CTA scans. However, the value of DLR can be increased by training the DCNN on more sophisticated teaching images. We expect that with DLR, the image quality can be improved at lower radiation exposure. Also, the training was performed by using clinical cardiac data only. If DLR algorithm is applied to other organs, individual training would be needed for each region, such as soft tissue, lung, and bone.

Table 1 Quantitative image quality parameters

	Hybrid IR	DLR	*p*
Image noise (HU)			
Ascending aorta	21.2 ± 4.1	18.3 ± 1.9	< 0.05
Left atrium	24.8 ± 3.8	19.5 ± 3.2	< 0.01
Septal wall of the ventricle	22.8 ± 5.1	17.5 ± 2.8	< 0.01
All locations	23.0 ± 4.6	18.5 ± 2.8	< 0.01
CNR in the LMA	22.8 ± 5.0	26.3 ± 3.1	< 0.01
CNR in the proximal RCA	23.3 ± 4.9	26.6 ± 3.8	< 0.01

Data are the mean ± standard deviation

DLR deep learning–based image restoration, *CNR* contrast-to-noise ratio, *LMA* left main artery, *RCA* right coronary artery

Table 2 Evaluation of the profile curves

	Hybrid IR	DLR	*p*
ERD_{mean} (mm)			
LMA	18.5 ± 3.1	16.2 ± 2.2	< 0.01
Proximal RCA	18.5 ± 2.9	16.7 ± 2.2	< 0.01
ERS_{mean} (HU/mm)			
LMA	21.1 ± 2.9	24.5 ± 3.4	< 0.01
Proximal RCA	21.4 ± 4.2	23.8 ± 4.4	< 0.01

Data are the mean ± standard deviation

DLR deep learning–based image restoration, *ERD* edge rise distance, *ERS* edge rise slope, *LMA* left main artery, *RCA* right coronary artery

Table 3 Visual evaluation of coronary arteries on hybrid IR and DLR images

	Score 1	Score 2	Score 3	Score 4	Total	Mean score
Hybrid IR	2	12	64	12	90	2.96
DLR	0	3	32	55	90	3.58

DLR deep learning–based image restoration

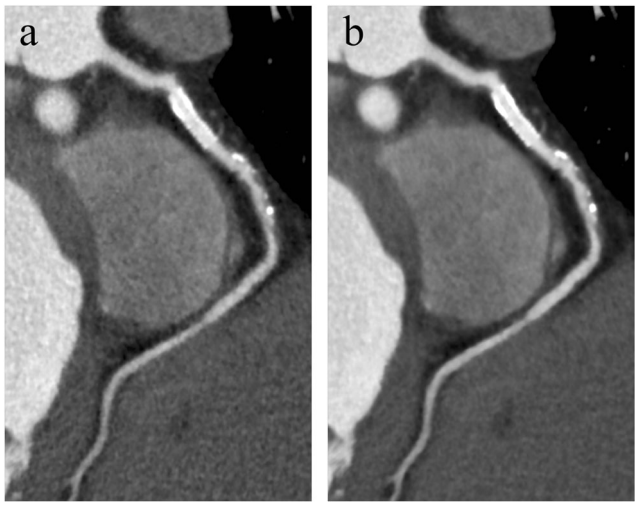

Fig. 6 A 61-year-old man with typical angina pectoris. Curved multiplanar reformation shows 50% stenosis of the mid-right coronary artery caused by predominantly noncalcified plaque, as well as more proximal nonobstructive stent. **a** Hybrid IR image (image noise, 24.4 HU; CNR, 19.4). The image quality was rated as good. **b** DLR image (image noise, 18.0 HU; CNR, 23.1). The image quality was rated as excellent

This study has some limitations. First, our study population was relatively small; additional investigations on larger cohorts are underway to confirm our preliminary results. Second, we evaluated the CT attenuation profiles selectively in the proximal RCA and LMA. We did not assess distal segments because their small diameter renders impossible the precise evaluation of the ERD and ERS. Third, coronary attenuation and the CNR were evaluated in only the proximal coronary arteries. The small diameter of distal segments makes it impossible to place ROIs that do not include parts of the vessel wall and adjacent tissue; this results in partial volume effects. Lastly, we did not confirm the diagnostic accuracy of our coronary CTA images by comparing our findings with invasive coronary angiography, the reference standard.

In conclusion, we report that the image noise was lower and the image quality was better on DLR than on hybrid IR at coronary CTA.

Funding The authors state that this work has not received any funding.

Compliance with ethical standards

Guarantor The scientific guarantor of this publication is Kazuo Awai.

Conflict of interest Kazuo Awai received a research grant from Canon Medical Systems Co. Ltd. Zhou Yu, Jian Zhou, and Yujie Lu are employees of Canon Medical Research USA. The other authors declare that they have no conflict of interest.

Statistics and biometry No complex statistical methods were necessary for this paper.

Informed consent Written informed consent was waived by the Institutional Review Board.

Ethical approval Institutional Review Board approval was obtained.

Methodology
- retrospective
- diagnostic or prognostic study
- performed at one institution

References

1. Raff GL, Gallagher MJ, O'Neill WW, Goldstein JA (2005) Diagnostic accuracy of noninvasive coronary angiography using 64-slice spiral computed tomography. J Am Coll Cardiol 46:552–557
2. Nikolaou K, Knez A, Rist C et al (2006) Accuracy of 64-MDCT in the diagnosis of ischemic heart disease. AJR Am J Roentgenol 187:111–117
3. Herzog C, Zwerner PL, Doll JR et al (2007) Significant coronary artery stenosis: comparison on per-patient and per-vessel or per-segment basis at 64-section CT angiography. Radiology 244:112–120
4. Dreyer KJ, Geis JR (2017) When machines think: radiology's next frontier. Radiology 285:713–718
5. Kahn CE Jr (2017) From images to actions: opportunities for artificial intelligence in radiology. Radiology 285:719–720
6. Chartrand G, Cheng PM, Vorontsov E et al (2017) Deep learning: a primer for radiologists. Radiographics 37:2113–2131
7. Anthimopoulos M, Christodoulidis S, Ebner L, Christe A, Mougiakakou S (2016) Lung pattern classification for interstitial lung diseases using a deep convolutional neural network. IEEE Trans Med Imaging 35:1207–1216
8. Becker AS, Marcon M, Ghafoor S, Wurnig MC, Frauenfelder T, Boss A (2017) Deep learning in mammography: diagnostic accuracy of a multipurpose image analysis software in the detection of breast cancer. Invest Radiol 52:434–440
9. Yoshida H, Nappi J (2007) CAD in CT colonography without and with oral contrast agents: progress and challenges. Comput Med Imaging Graph 31:267–284
10. Bauer S, Wiest R, Nolte LP, Reyes M (2013) A survey of MRI-based medical image analysis for brain tumor studies. Phys Med Biol 58:R97–R129
11. Chen H, Zhang Y, Zhang W et al (2017) Low-dose CT via convolutional neural network. Biomed Opt Express 8:679–694
12. Yang Q, Yan P, Zhang Y et al (2018) Low-dose CT image denoising using a generative adversarial network with Wasserstein distance and perceptual loss. IEEE Trans Med Imaging 37:1348–1357
13. Fan Y, Zamyatin A, Nakanishi S (2012) Noise simulation for low-dose computed tomography. 2012 IEEE Nuclear Science Symposium and Medical Imaging Conference Record (NSS/MIC), Anaheim, CA, pp 3641–3643
14. Hausleiter J, Meyer T, Hermann F et al (2009) Estimated radiation dose associated with cardiac CT angiography. JAMA 301:500–507
15. Lembcke A, Wiese TH, Schnorr J et al (2004) Image quality of noninvasive coronary angiography using multislice spiral computed tomography and electron-beam computed tomography: intraindividual comparison in an animal model. Invest Radiol 39:357–364
16. Tatsugami F, Husmann L, Herzog BA et al (2009) Evaluation of a body mass index-adapted protocol for low-dose 64-MDCT coronary angiography with prospective ECG triggering. AJR Am J Roentgenol 192:635–638
17. Tatsugami F, Higaki T, Sakane H et al (2017) Coronary artery stent evaluation with model-based iterative reconstruction at coronary CT angiography. Acad Radiol 24:975–981

18. Nelson RC, Feuerlein S, Boll DT (2011) New iterative reconstruction techniques for cardiovascular computed tomography: how do they work, and what are the advantages and disadvantages? J Cardiovasc Comput Tomogr 5:286–292
19. Geyer LL, Schoepf UJ, Meinel FG et al (2015) State of the art: iterative CT reconstruction techniques. Radiology 276:339–357
20. Birnbaum BA, Hindman N, Lee J, Babb JS (2007) Multi-detector row CT attenuation measurements: assessment of intra- and interscanner variability with an anthropomorphic body CT phantom. Radiology 242:109–119
21. Suzuki S, Machida H, Tanaka I, Ueno E (2013) Vascular diameter measurement in CT angiography: comparison of model-based iterative reconstruction and standard filtered back projection algorithms in vitro. AJR Am J Roentgenol 200:652–657
22. Yokomachi K, Tatsugami F, Higaki T et al (2018) Neointimal formation after carotid artery stenting: phantom and clinical evaluation of model-based iterative reconstruction (MBIR). Eur Radiol. https://doi.org/10.1007/s00330-018-5598-5